

# Arousal and Locomotion Make Distinct Contributions to Cortical Activity Patterns and Visual Encoding

## Highlights

- Behavioral state transitions reveal epochs of arousal without locomotion
- Isolated arousal is linked with suppressed firing rates and altered LFP activity
- Locomotion is associated with elevated visual cortex firing rates
- Arousal mediates enhanced visual processing

## Authors

Martin Vinck, Renata Batista-Brito, Ulf Knoblich, Jessica A. Cardin

## Correspondence

jess.cardin@yale.edu

## In Brief

Spontaneous and sensory-evoked brain activity varies with behavior, but the contributions of arousal state and motor activity to these changes remain unclear. Vinck et al. identify separate roles of arousal and locomotion in regulating sensory processing in visual cortex.



# Arousal and Locomotion Make Distinct Contributions to Cortical Activity Patterns and Visual Encoding

Martin Vinck,<sup>1,3</sup> Renata Batista-Brito,<sup>1,3</sup> Ulf Knoblich,<sup>1,4</sup> and Jessica A. Cardin<sup>1,2,\*</sup>

<sup>1</sup>Department of Neurobiology, Yale University School of Medicine, 333 Cedar Street, New Haven, CT 06520, USA

<sup>2</sup>Kavli Institute of Neuroscience, Yale University, 333 Cedar Street, New Haven, CT 06520, USA

<sup>3</sup>Co-first author

<sup>4</sup>Present address: Allen Brain Institute, 551 N. 34<sup>th</sup> Street, Seattle, WA 98103, USA

\*Correspondence: [jess.cardin@yale.edu](mailto:jess.cardin@yale.edu)

<http://dx.doi.org/10.1016/j.neuron.2015.03.028>

## SUMMARY

Spontaneous and sensory-evoked cortical activity is highly state-dependent, yet relatively little is known about transitions between distinct waking states. Patterns of activity in mouse V1 differ dramatically between quiescence and locomotion, but this difference could be explained by either motor feedback or a change in arousal levels. We recorded single cells and local field potentials from area V1 in mice head-fixed on a running wheel and monitored pupil diameter to assay arousal. Using naturally occurring and induced state transitions, we dissociated arousal and locomotion effects in V1. Arousal suppressed spontaneous firing and strongly altered the temporal patterning of population activity. Moreover, heightened arousal increased the signal-to-noise ratio of visual responses and reduced noise correlations. In contrast, increased firing in anticipation of and during movement was attributable to locomotion effects. Our findings suggest complementary roles of arousal and locomotion in promoting functional flexibility in cortical circuits.

## INTRODUCTION

Patterns of cortical activity differ dramatically across behavioral states, such as sleeping, anesthesia, and waking (Berger, 1929; Haider et al., 2013; Steriade et al., 1993; Steriade et al., 2001). Likewise, neural responses to sensory inputs depend strongly on ongoing patterns of internally generated activity (Civillico and Contreras, 2012; Hasenstaub et al., 2007; Livingstone and Hubel, 1981). The generation of multiple activity patterns associated with sleep and anesthesia states has been examined in great detail (Berger, 1929; Contreras et al., 1996; Destexhe et al., 1999; McCormick and Bal, 1997; Steriade et al., 1993, 2001). However, relatively little is known about transitions between distinct waking states, such as quiescence, arousal, and focused attention.

Recent studies in rodents have contrasted inactive versus active behavioral states, in particular quiescent versus whisk-

ing (Crochet and Petersen, 2006; Gentet et al., 2010; Zagha et al., 2013) or running (Bennett et al., 2013; Fu et al., 2014; Keller et al., 2012; Niell and Stryker, 2010; Polack et al., 2013; Reimer et al., 2014; Saleem et al., 2013; Schneider et al., 2014; Zhou et al., 2014), and found profound differences in cortical activity patterns that resemble the effects of focused spatial attention in primates (Cohen and Maunsell, 2009; Fries et al., 2001; Harris and Thiele, 2011; McAdams and Maunsell, 1999; Mitchell et al., 2009). In mouse primary visual cortex (V1), locomotion is accompanied by altered firing rates, a reduction in low-frequency fluctuations in the membrane potential and local field potential (LFP), and an increase in LFP gamma-band oscillations (Keller et al., 2012; Niell and Stryker, 2010; Polack et al., 2013; Reimer et al., 2014; Saleem et al., 2013). Enhanced firing rates during locomotion are particularly prominent in inhibitory interneurons (Bennett et al., 2013; Fu et al., 2014; Niell and Stryker, 2010; Polack et al., 2013; Reimer et al., 2014). Locomotion is also associated with an increase in the gain of visual responses (Bennett et al., 2013; Niell and Stryker, 2010; Polack et al., 2013; Reimer et al., 2014).

Because the most commonly studied active states involve a substantial motor component, it remains unclear whether the associated changes in cortical activity patterns are specific to motor output or more generally attributable to changes in global arousal. Recordings during manipulations of the visual environment suggest that much of the change in firing rates during locomotion is consistent with multimodal processing of visual and motor signals (Keller et al., 2012; Saleem et al., 2013). The integration of locomotor and visual signals in V1 may thus represent elements of predictive coding or play a role in spatial navigation. However, locomotion-associated changes in cortical activity have been replicated by noradrenergic and cholinergic manipulations in the absence of motor output (Fu et al., 2014; Lee et al., 2014; Polack et al., 2013). Changes in V1 activity during locomotion may therefore result from recruitment of neuromodulatory systems that regulate global arousal levels.

Wakefulness comprises states of low and high arousal, but the relationship between changes in arousal and cortical activity remains poorly understood. The functional impact of motor feedback signals to sensory cortex is likewise only beginning to be explored (Guo et al., 2014; Lee et al., 2013; Schneider et al., 2014; Zagha et al., 2013). Here we used behavioral state monitoring and manipulation to dissociate the roles of locomotion and arousal in regulating neural activity in mouse V1. We

recorded from V1 in mice head-fixed on a wheel to measure locomotion and monitored pupil diameter to assess arousal (Ashton-Jones and Cohen, 2005; Eldar et al., 2013; Gilzenrat et al., 2010; Reimer et al., 2014). To disentangle the effects of motor activity and arousal, we first took advantage of naturally occurring state transitions where mice initiated or finished a bout of locomotion. We examined the precise time course of changes in the LFP, single-unit firing rates, and pupil diameter around locomotion onset and offset. We further compared epochs of high and low arousal during quiescent states. In a second set of experiments, we causally manipulated behavioral state and induced a shift from low to high arousal in the absence of locomotion by delivering an air puff to the animal's body. We find that arousal mediates most state-dependent changes in LFP activity, whereas increases in overall firing rates are attributable to locomotion. In contrast, enhancement of visual encoding during locomotion is associated with increased arousal, rather than motor activity.

## RESULTS

### Dissociating Locomotion and Arousal

To separate the contributions of locomotion and arousal to V1 activity and visual encoding, we performed simultaneous recordings of isolated single units and LFPs from multiple sites throughout layers 2–6 of V1 in awake mice (Figure 1;  $n = 88$  sessions in 28 mice). Mice were head-fixed on a spring-mounted wheel apparatus (Figure S1A) and recordings were made during both baseline and visual stimulation periods. Behavioral state was assessed by continuous monitoring of arousal and locomotion. To monitor arousal, we measured pupil dilation in the eye that was contralateral to the visual stimulus (Figure 1A; Movie S1). Transition points were defined as shifts from quiescence (used synonymously with sitting) to locomotion or from locomotion to quiescence and were identified by detecting significant changes in the statistics of the locomotion speed signal from the wheel with high temporal resolution (Figure 1B).

We found complex temporal relationships among pupil diameter, locomotion, LFP dynamics, and the firing rates of V1 neurons (Figure 1A). At locomotion onset, speed rapidly increased, reaching a plateau after about 2.5 s and remaining at  $\sim 10$ –15 cm/s until just prior to locomotion offset (Figure 1B). Locomotion speed and pupil diameter were consistently correlated at transition points. Pupil diameter increased prior to the onset of locomotion, suggesting that arousal reliably preceded movement. Pupil diameter reached a plateau after about 2.5 s, and remained elevated until locomotion offset (Figure 1C). Locomotion offset was followed by a gradual decrease in pupil diameter that did not reach baseline values until 40 s later (Figure 1C), indicating a substantial period of elevated arousal in the absence of locomotion. Periods of high arousal and locomotion thus occurred both together and separately, allowing us to discriminate their roles in regulating V1 activity.

### LFP Modulation by Behavioral State Transition

To dissociate LFP changes associated with locomotion and arousal, we computed time-frequency representations of LFP signals around locomotion onset and offset in the absence of vi-

sual stimuli. Locomotion onset was preceded by a sharp increase in spontaneous LFP gamma oscillations (55–65 Hz) and a decrease in low-frequency LFP fluctuations (1–4 Hz; Figure 2A). Gamma power decreased gradually over time after locomotion onset, whereas low-frequency fluctuations remained suppressed throughout the locomotion period (Figure 2A). In contrast, locomotion offset was followed by a gradual increase in low-frequency LFP power and a gradual decrease in LFP gamma power that lasted up to 40–50 s (Figure 2B). The time courses of LFP low frequency and gamma power were strongly correlated (Spearman correlation) with the time course of pupil dynamics, but not with the time course of locomotion speed (Figure 2C). The correlations between LFP power and pupil diameter time courses were strongly linear (gamma and pupil: Pearson's  $R = 0.94$ ,  $p = 0.0000024$ ; 1–4 Hz and pupil: Pearson's  $R = -0.93$ ,  $p = 0.000041$ ), suggesting that arousal, rather than locomotion, mediates most of the observed change in LFP patterns.

We also recorded LFP activity in V1 while presenting visual stimuli. All stimuli were drifting gratings on a mean luminance background (see Experimental Procedures). We found that the increase in LFP gamma-band power and decrease in low-frequency power during locomotion periods were observed for both visual stimulation and inter-trial interval (ITI) epochs (Figure 2D), in congruence with previous findings that locomotion without visual stimulation correlates with increased gamma power (Niell and Stryker, 2010). Visual stimulation during locomotion caused an increase in gamma band power at frequencies above 60 Hz, with a spectral peak around 75 Hz (Figure 2E). During quiescent periods, visual stimulation instead caused an increase in gamma-band power at a broader range above 20 Hz, with a relatively shallow spectral peak around 30 Hz (Figure 2E). We further found that contrast tuning of LFP gamma-band power was affected by locomotion, with increased and decreased gain at high and low gamma frequencies, respectively (Figure S2).

To examine how LFP fluctuations related to local V1 spiking activity, we computed the strength of spike-LFP phase-locking for 34 FS (11 in L2/3, 23 in L5/6) and 157 RS (31 in L2/3, 126 in L5/6) cells that were classified based on action potential waveform characteristics (Figures S1C–S1F). Locomotion increased gamma phase-locking and decreased low-frequency phase-locking for both RS and FS cells (Figure 2F). Gamma phase-locking was stronger for FS than RS cells during periods of both quiescence and locomotion (Figure 2F).

### Cell-Type-Specific Modulation of Firing Rates

Next, we investigated the contributions of locomotion and arousal to V1 firing rates in the absence of visual stimuli. We compared firing rates between epochs of locomotion and quiescence and within each type of epoch to examine the temporal dynamics of changes in firing around transition points (Figure 3A). Individual V1 neurons demonstrated a broad range of relationships between spontaneous firing rate and behavioral state (Figure 3A; Figure S3A). Both FS and RS cells' spontaneous firing rates increased before locomotion onset, peaked around the time of locomotion onset, and declined over time throughout the locomotion period (Figures 3A and 3B). To quantify the anticipatory effect for individual cells, we computed the Pearson cross-correlation coefficient between locomotion speed and

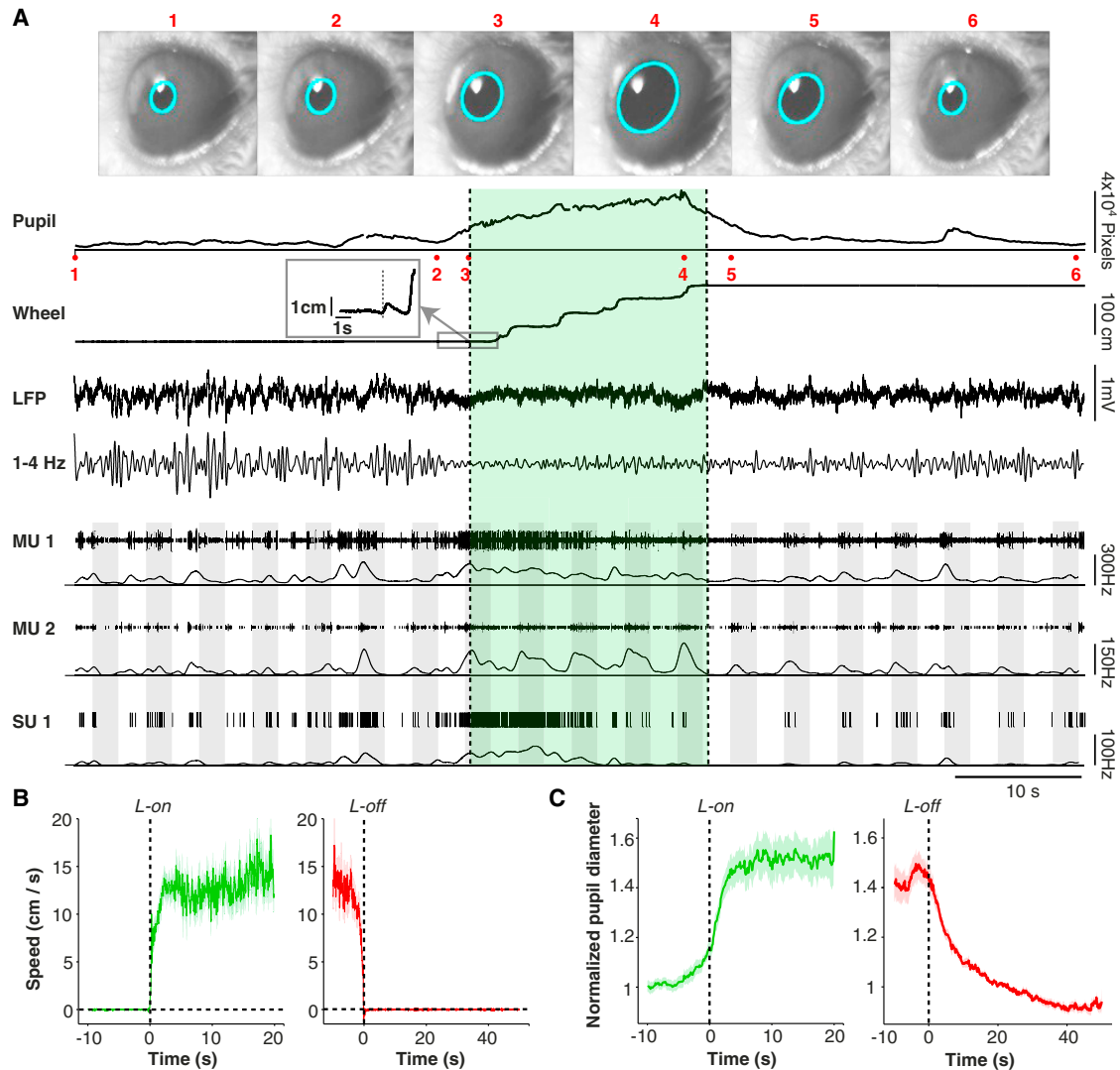


**Figure 1. Experimental Paradigm to Separate the Contributions of Arousal and Locomotion to Neural Activity and Visual Encoding in V1**

(A) Example data from one experimental session. Video frame images of the mouse's eye (1–6) are shown where acquired at the times indicated in the pupil recording trace. Pupil diameter (PD) was recorded on video and extracted posthoc via a fitted ellipse (cyan). The average pupil diameter in pixel units is shown as a function of time. Locomotion is shown as a linearized version of the wheel position. Locomotion onset point is shown in the inset. The locomotion period is indicated by green shading. LFP recording is shown as a raw broadband LFP signal for a superficial electrode, together with the 1–4 Hz filtered signals. Thresholded multi-unit traces and spike densities (1 s Gaussian smoothing kernel with SD of 0.25 s) are shown for a superficial (MU1) and deep (MU2) electrode, respectively, together with a single unit trace that was isolated from MU1. Grey shadings indicate visual stimuli at 100% contrast and varying orientations.

(B) Locomotion speed around locomotion onset (green) and offset (red), shown as mean  $\pm$  SEM (across sessions).

(C) Population average pupil diameter, normalized to PD at 20–25 s point after locomotion offset, as a function of time around locomotion onset (green) and offset (red), shown as mean  $\pm$  SEM.

instantaneous firing rate in the interval around locomotion onset. Most cells exhibited a strong linear correlation between locomotion speed and firing rate that was forward-shifted in time, indicating that increases in RS and FS firing rates preceded increases in locomotion speed (Figures S3B and S3C).

Both FS and RS firing rates were significantly higher during the early period around locomotion onset (within  $\pm 1$  s of locomotion onset; LE) than during the late locomotion period ( $>10$  s after locomotion onset; LL) (Figure 3C; Figure S4A). To directly compare locomotion-related changes between RS and FS cells,

we computed a rate modulation value  $(FR_b - FR_a)/(FR_a + FR_b)$ , which normalizes for absolute rate differences. RS and FS cells exhibited similar degrees of rate modulation during the early versus the late locomotion period ( $p = 0.48$ ; Figure 3D). We did not observe a significant difference in LE versus LL rate modulation between cells recorded from superficial and deep layers (RS L2/3:  $0.16 \pm 0.092$ , L5/6:  $0.22 \pm 0.041$ ,  $p = 0.72$ ; FS L2/3:  $0.30 \pm 0.21$ , L5/6:  $0.32 \pm 0.068$ ,  $p = 0.93$ ). We found no significant difference between unclassified single (US) units (Figures S1C–S1F) and RS cells (US:  $0.22 \pm 0.08$ ,  $p = 0.96$ ).

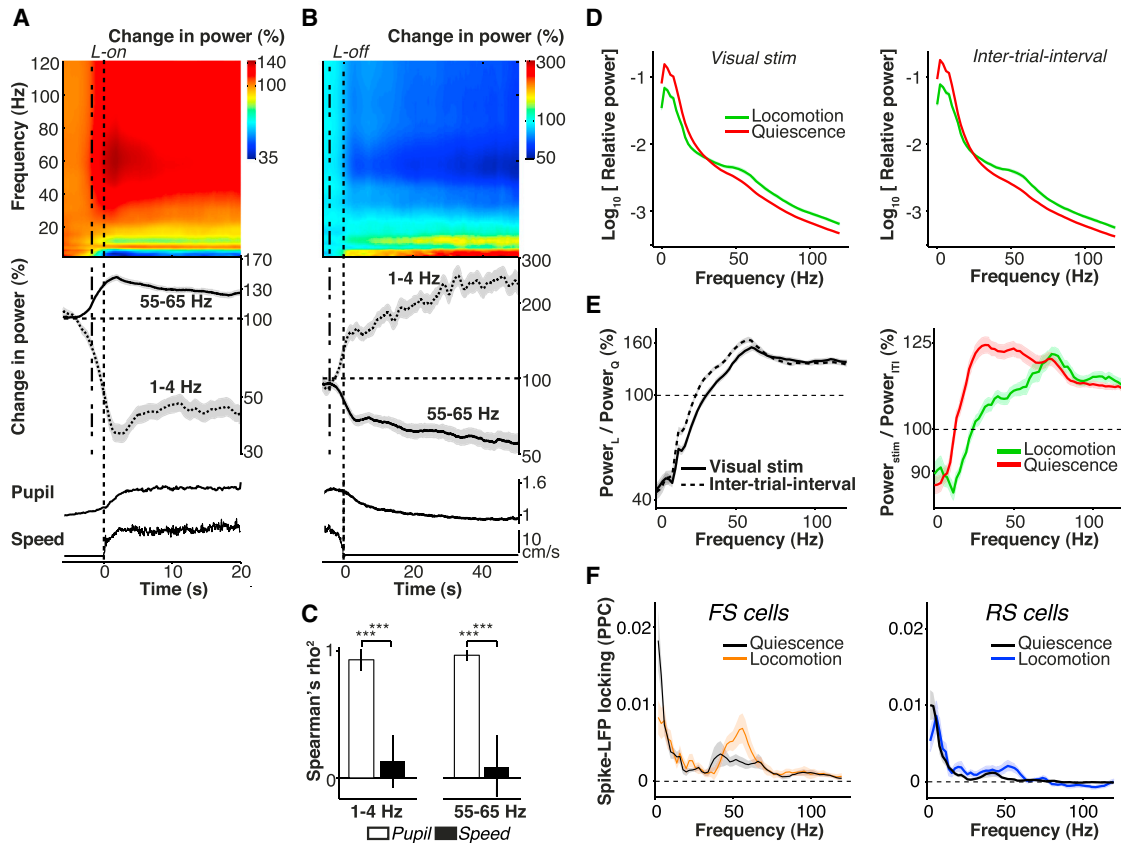


**Figure 2. Contributions of Arousal and Locomotion to V1 LFP Rhythms**

(A) Top: time-frequency representation of LFP signals around locomotion onset (L-on), showing base-10 log-transformed relative power, i.e., power at time  $t$  divided by average power in the quiescent interval preceding L-on ( $-4.5$  to  $-4$  s). Power was computed in sliding windows of  $\pm 2$  s using short-term Fourier transform. Log power ratios are shown as percentages. Middle: Line plots of gamma (55–65 Hz) and low-frequency (1–4 Hz) power across  $n = 58$  sites in 11 mice, shown as mean  $\pm$  SEM. Dashed lines at 2 s before zero represent the effective time at which data after L-on would be included in computation, revealing spectral changes before this point. Note the appearance of an 8–10 Hz theta-band that interrupts the reduction in low-frequency LFP fluctuations, presumably due to volume conduction from the hippocampus. Bottom: pupil and wheel traces, as in Figures 1B and 1C.

(B) As (A), but now for L-off. Relative power was computed by dividing by the average power in the epoch before locomotion offset ( $-3$  to  $-2.5$  s), for  $n = 133$  sites in 18 mice.

(C) Spearman's correlation (shown the square of the Spearman's rho) between either average pupil diameter (PD) (open bars) or locomotion speed (closed bars) with average gamma and delta time courses for quiescence period, using data  $> -3$  s before locomotion offset till 40 s after locomotion offset. \*\*\* $p < 0.001$ . Shown mean  $\pm$  SEM.  $n = 133$  sites in 18 mice.

(D) Average power spectra during visual stimulation period (left) and ITI (right), separately for locomotion and quiescent periods, for  $n = 196$  sites in 23 mice. Power spectra were computed using multitapering of 500 ms windows, with a smoothing window of  $\pm 4$  Hz.

(E) Left: base-10 log-transformed ratio of spectral power during locomotion over quiescence, separated for visual stimulation and ITI periods, shown as a percentage. Right: base-10 log-transformed ratio of spectral power during visual stimulation over ITI period, separated for locomotion and quiescence, shown as a percentage.

(F) Spike-field locking spectra (PPC) for FS (left) and RS (right) cells, separately for locomotion and quiescence periods. Shadings correspond to SEMs across cells. The difference between locomotion and quiescence was significant at both 2 Hz and 60 Hz for FS and RS cells ( $p < 0.05$ , bootstrap test on mean PPC). The difference between RS and FS was significant at 60 Hz for both locomotion and quiescence ( $p < 0.05$ , randomization test on means). FS: 25/12; RS: 61/18 (#cells/#mice).

We next examined whether increases in firing rate in anticipation of and during locomotion might be explained by the associated change in arousal. The increase in firing rate before locomotion might be attributable to an increase in arousal, since pupil dilation precedes locomotion onset, or may alternatively reflect a preparatory phase in advance of motor execution. To separate the effects of locomotion and arousal, we therefore examined the trajectories of firing rates during quiescence following locomotion

offset, when pupil diameter showed substantial variation in the absence of movement (Figures 1B and 1C). For both RS and FS cells, locomotion offset was accompanied by a rapid decrease in firing rates, followed by a subsequent gradual increase over time (Figure 3A). Thus, a state of heightened arousal, corresponding to maintained pupil dilation after the cessation of movement, is accompanied by decreased rather than increased RS and FS firing.

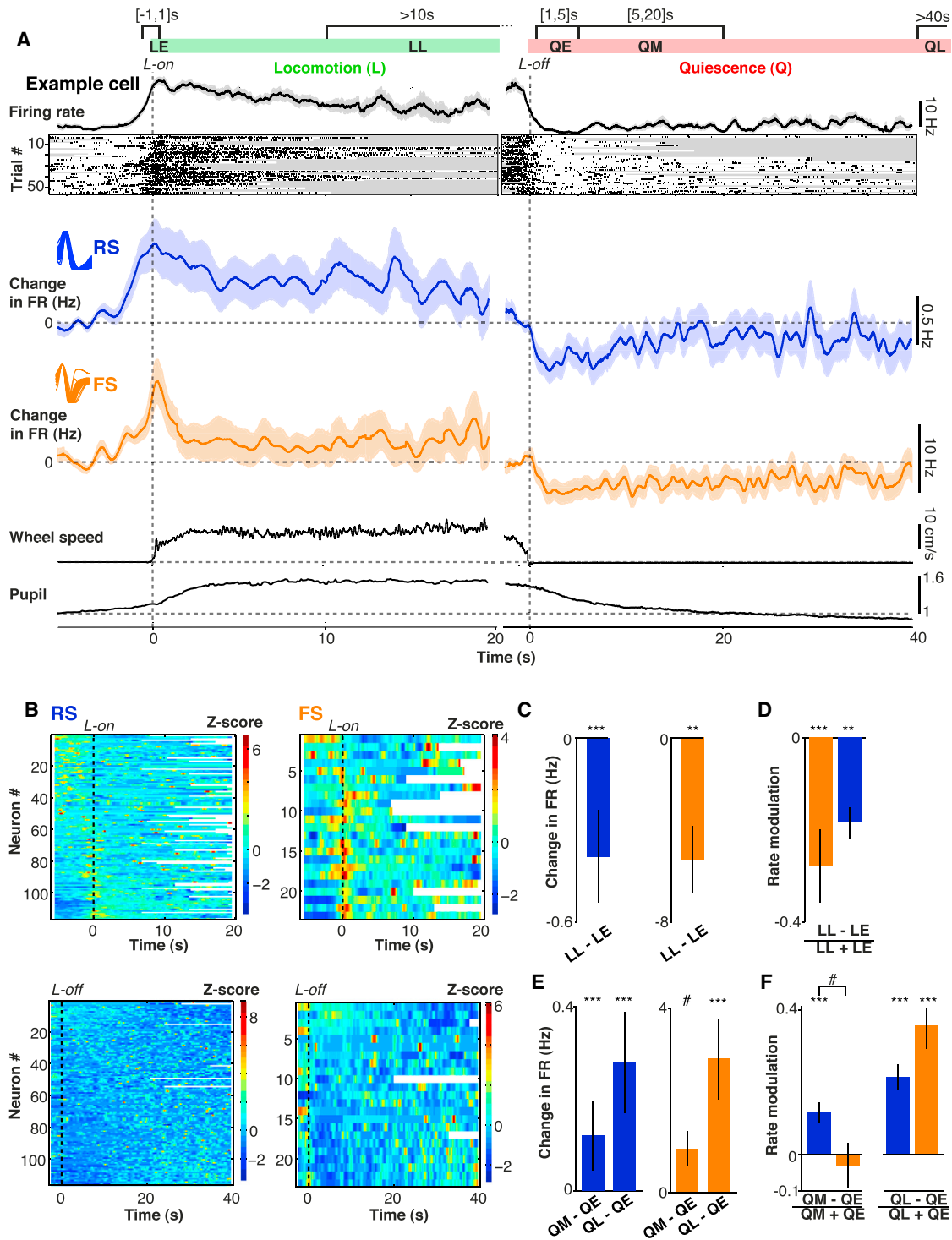


**Figure 3. Contributions of Arousal and Locomotion to Spontaneous Firing Activity in V1**

(A) Schematic showing division of data into epochs for analysis. LE: early locomotion period (–1 to 1 s around L-on). LL: late locomotion period (>10 s after L-on). QE: early quiescent period (1–5 s after L-off). QM: middle quiescent period (5–20 s after L-off). QL: late quiescent period (>40 s after L-off). Plots show firing rate for an example FS cell during locomotion onset (L-on, left) and locomotion offset (L-off, right). Rasters show individual transition points for the same cell. Gray shadings indicate L-off and L-on during individual trials. Next, shown (left) the average (mean  $\pm$  SEM) change in RS (blue) and FS (orange) cells' firing rates relative to a quiescent baseline period (taken –6 to –3 s before L-on) as a function of time, and (right) the change in firing rates relative to a baseline locomotion period (defined –3 to –1 s before L-off) as a function of time around L-off. Insets show average waveforms for RS and FS cells, as in Figure S1C. Bottom: pupil and wheel traces, as in Figures 1B and 1C.

(legend continued on next page)

To directly compare firing rates across epochs within the quiescent period, we analyzed early quiescence (1–5 s after locomotion offset; QE), middle quiescence (5–20 s after locomotion offset; QM) and late quiescence (>40 s after locomotion offset; QL) (Figure 3A). Pupil diameter was significantly decreased across the QE to QM to QL intervals after locomotion offset (Figure S4E). In contrast, FS and RS firing rates significantly increased across the QE to QM to QL intervals after locomotion offset (Figures 3E and 3F). We found no significant difference in rate modulation between FS and RS cells across quiescent epochs (Figures 3E and 3F). We did not observe a significant difference in rate modulation between QE and QL intervals when comparing cells recorded from superficial and deep layers (RS L2/3:  $-0.23 \pm 0.10$ , L5/6:  $-0.21 \pm 0.037$ ,  $p = 0.64$ ; FS L2/3:  $-0.41 \pm 0.13$ , L5/6:  $-0.33 \pm 0.079$ ,  $p = 1$ ). No significant difference was observed between RS and US cells (US:  $-0.10 \pm 0.06$ ,  $p = 0.12$ ).

To further quantify the trajectory of V1 firing rates over time, we computed Spearman correlation coefficients between firing rate and time after locomotion offset (using only data >3 s after locomotion offset; Experimental Procedures). Many cells showed a significant association between firing rate and time (FS: 10/23, RS: 37/80, at  $p < 0.05$ ), and the average correlation was higher than zero (Figure S4B, mean  $\pm$  SEM of Spearman's  $\rho = 0.04 \pm 0.024$ ,  $p = 0.034$ ; Rank-Wilcoxon test). However, we also found subpopulations of cells whose firing rate either decreased or increased over time (Figure 3B; Figure S4B, FS positive: 6/23, negative: 4/23; RS positive: 20/80, negative: 17/80,  $p < 0.05$ ), suggesting diverse firing rate trajectories across the V1 population.

Figure 3B shows a subset of RS and FS cells whose firing rates were lower during locomotion than during quiescence. This suppression effect was also observed when we excluded the 20 s of data immediately before locomotion onset, indicating that it was not an artifact of anticipatory firing (Figures S4C and S4D). To investigate whether this suppressive effect was due to arousal or locomotion, we compared the locomotion period with either the entire quiescent period, which is overall associated with low arousal levels, or with the early quiescent period, which is characterized by high arousal levels. Despite showing suppression during locomotion relative to the entire quiescent period, this subset of cells showed no suppression when we restricted the comparison to the early quiescent period (Figures S4C and S4D). This suggests that the locomotion-associated firing reduction in this subset of cells is likely due to the suppressive effect of arousal, rather than locomotion. Overall, our results indicate that both RS and FS cells in V1 demonstrate increased spontaneous activity in anticipation of and during locomotion. However, a state of heightened arousal, as indicated by maintained pupil dilation after the cessation of move-

ment, is accompanied by a decrease in spontaneous RS and FS firing. In contrast to the spectral changes in LFP signals, elevated firing during movement is thus specific to locomotion periods and unlikely to result from associated changes in global arousal.

### Modulation of Visual Encoding by State Transition

To determine the impact of locomotion and arousal on visual encoding, we recorded unit activity in V1 while presenting visual stimuli. The robust differences in visually evoked LFP dynamics between periods of locomotion and quiescence (Figure 2; Figure S2) suggest that visual stimulation may likewise differentially affect firing rates during these states. We therefore computed the mean peak firing rate of cells in response to stimuli presented during locomotion and quiescence (Figures 4A and 4B; Figure S5A). To separate the effects of locomotion and arousal, we divided the quiescence period into separate epochs as in Figure 3. The exact durations of the epochs were adjusted to account for the duration and timing of stimulus presentation. We analyzed early quiescence (3–20 s after locomotion offset; QE), when the pupil was relatively dilated, and late quiescence (>40 s after locomotion offset; QL), when the pupil was relatively constricted. We used a signal-to-noise (SNR) ratio index (SNRI), defined as  $(FR_{stim} - FR_{ITI}) / (FR_{stim} + FR_{ITI})$ , to assess visual encoding by V1 neurons during each epoch (as shown in the Experimental Procedures, the SNRI corresponds to a monotonic sigmoid transformation of the  $SNR = FR_{stim} / FR_{ITI}$ , mapping the SNR onto the  $-1$  to  $1$  interval). We found an overall increase in the SNRI of visual encoding during locomotion in comparison to quiescence for RS, but not FS, cells (Figure 4C). A finer analysis of time periods found that the SNRI in early quiescence (QE), during high arousal, was larger than in late quiescence (QL), during low arousal, for both RS and FS cells (Figure 4C). The SNRI in the quiescent period 20–40 s after locomotion offset reached intermediate values for both FS and RS cells (RS:  $0.16 \pm 0.044$ , FS:  $0.35 \pm 0.054$ ). We found that spontaneous, but not visually evoked, RS firing rates were significantly higher in the late than in the early quiescence period (Figures S5B–S5D). The observed increase in signal-to-noise ratio during high arousal states thus largely resulted from the differential effects of arousal on spontaneous and evoked firing rates.

The SNRI is a measure of the encoding of visual stimuli by individual neurons. However, visual stimuli are likely to be encoded by patterns of V1 population activity (Olshausen and Field, 1996; Pouget et al., 2000). We therefore calculated noise correlations, which may determine the efficiency of population coding (Cohen and Kohn, 2011; Ecker et al., 2010), for each epoch (Experimental Procedures). Overall, noise correlations were significantly lower during periods of locomotion than during quiescence (Figures 4D and 4E). Because low-frequency and

(B) Upper: overview of all recorded RS (left) and FS (right) cells, sorted by firing rate difference between quiescent baseline and the interval around L-on ( $-1$  to  $1$  s). Color coding corresponds to Z-scored firing rates. For each cell, Z scoring was performed over the mean change in firing rate in the shown interval. Lower: as in the upper image, but as a function of time around L-off and sorted on Spearman's correlation between time after L-off (>3 s) and quiescence. (C and D) Mean  $\pm$  SEM. of firing rate differences (C) and firing rate modulation (D) between LE and LL epochs. Statistical testing using two-sided Rank-Wilcoxon tests. # $p < 0.1$ , \* $p < 0.05$ , \*\* $p < 0.01$ , \*\*\* $p < 0.001$ . RS:  $n = 106/17$ ; FS:  $n = 18/9$ . (E and F) As in (C) and (D), but now for QE versus QL and QM versus QL. RS: 101/18, 101/18, FS: 21/10, 18/9 (#cells/#mice). Statistical comparison of QM versus QL rate modulation: RS, FS:  $p = 0.00071, 0.00086$ .

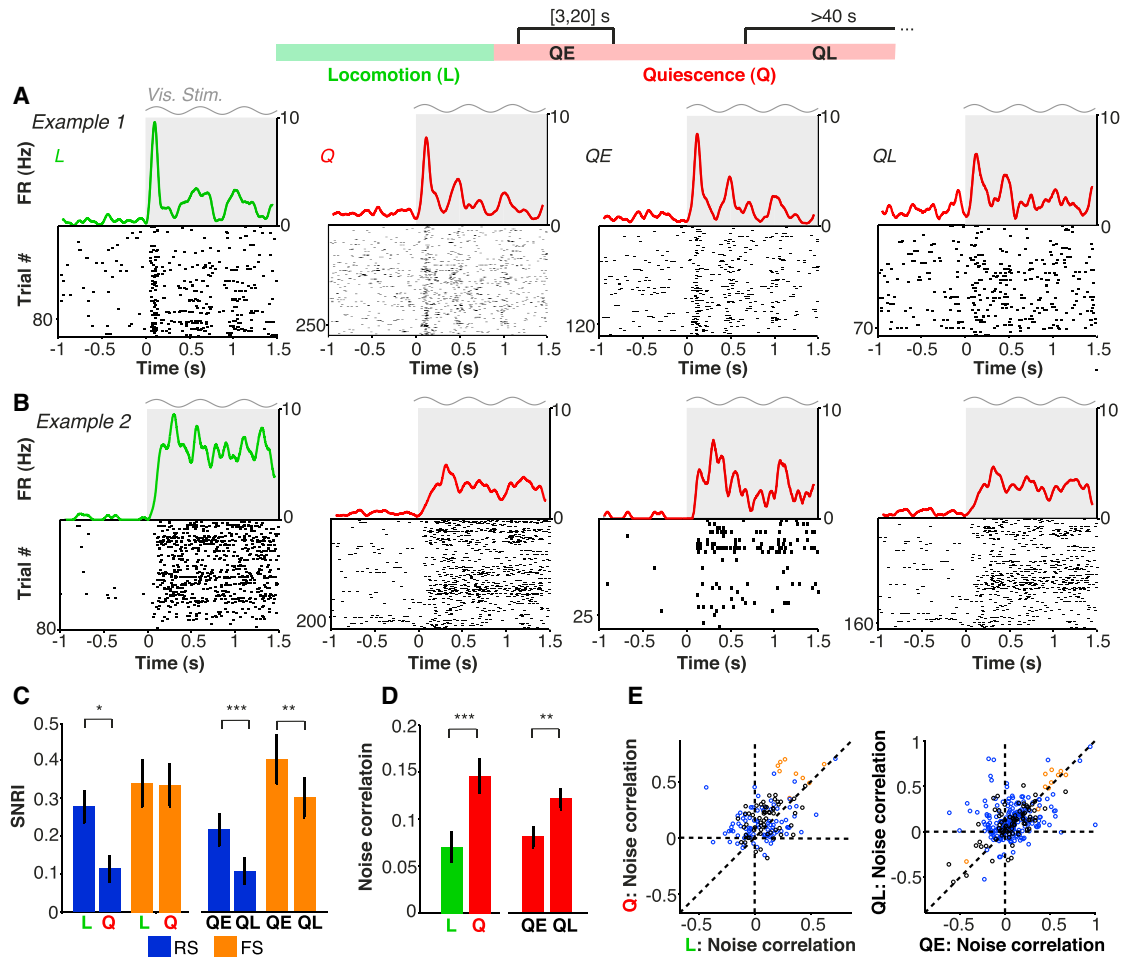


**Figure 4. Contributions of Locomotion and Arousal to Visual Encoding and Noise Correlations in V1**

(A and B) Raster plots of the visual responses of two example RS cells with associated firing rate density (computed using  $\pm 0.025$  s Gaussian kernels with SD of 0.0125 s) for all locomotion (L), all quiescence (Q), early quiescence (QE; 3–20 s after locomotion offset) and late quiescence (QL; >40 s after locomotion offset). Gray shading and sinusoid indicate visual stimulation.

(C) Mean  $\pm$  SEM of signal-to-noise ratio (SNRI), defined as  $(FR_{stim} - FR_{T1}) / (FR_{stim} + FR_{T1})$ , for each period. # $p < 0.1$ , \* $p < 0.05$ , \*\* $p < 0.01$ , \*\*\* $p < 0.001$ , two-sided Rank-Wilcoxon test. RS:  $n = 88/20$  (Q-L), 101/20 (QE, QL); FS:  $n = 23/10$ , 24/11 (#cells/#mice). Note that values for Q are closer to those for QL because more stimulus repetitions were available for QL.

(D) Mean  $\pm$  SEM of noise correlation of firing rates during different behavioral periods.  $n = 155/9$ , 289/11 (#pairs/#mice). \* $p < 0.05$ , \*\* $p < 0.01$ , \*\*\* $p < 0.001$ , two-sided Rank-Wilcoxon test.

(E) Left: noise correlation for locomotion versus quiescence. Circles correspond to cell pairs. FS-FS:  $n = 9/3$ ; RS-RS: 90/7; FS-RS (black):  $n = 56/5$ . Right: as left, but for QE versus QL. FS-FS: 10/4; RS-RS: 206/7; FS-RS:  $n = 73/7$ .

gamma-band LFP power showed gradual changes over time after locomotion offset, we hypothesized that noise correlations would increase with time after locomotion offset. Indeed, noise correlations were significantly elevated during late quiescent periods, when arousal was low, as compared to early quiescent periods (Figures 4D and 4E).

These results suggest that visual encoding is enhanced during locomotion because of increased signal-to-noise ratio and decorrelation of visually evoked activity. However, these changes are mainly attributable to arousal, rather than locomotion, as comparable changes in signal-to-noise ratio and noise correlations were observed during periods of heightened arousal in the absence of movement.

### Isolating the Cortical Effects of Arousal

The analyses of naturally occurring state transitions described above suggest separable effects of locomotion and arousal on firing rates, LFP activity, and visual encoding in V1. However, it is possible that the period of heightened arousal following locomotion offset represents an unusual form of arousal or is affected by long-lasting modulation of V1 activity by motor signals. To more causally test the role of arousal in regulating neural activity, we induced a state of enhanced arousal by puffing air on the back of the mouse (Figure S1B; Experimental Procedures). In a subset of sessions ( $n = 20$  sessions in ten mice), we administered brief air puffs (mean  $\pm$  SEM of rate =  $0.0089 \pm 0.0018$  Hz, mean  $\pm$  SEM of air puff number =  $42.23 \pm 5.63$ ) to the mouse while

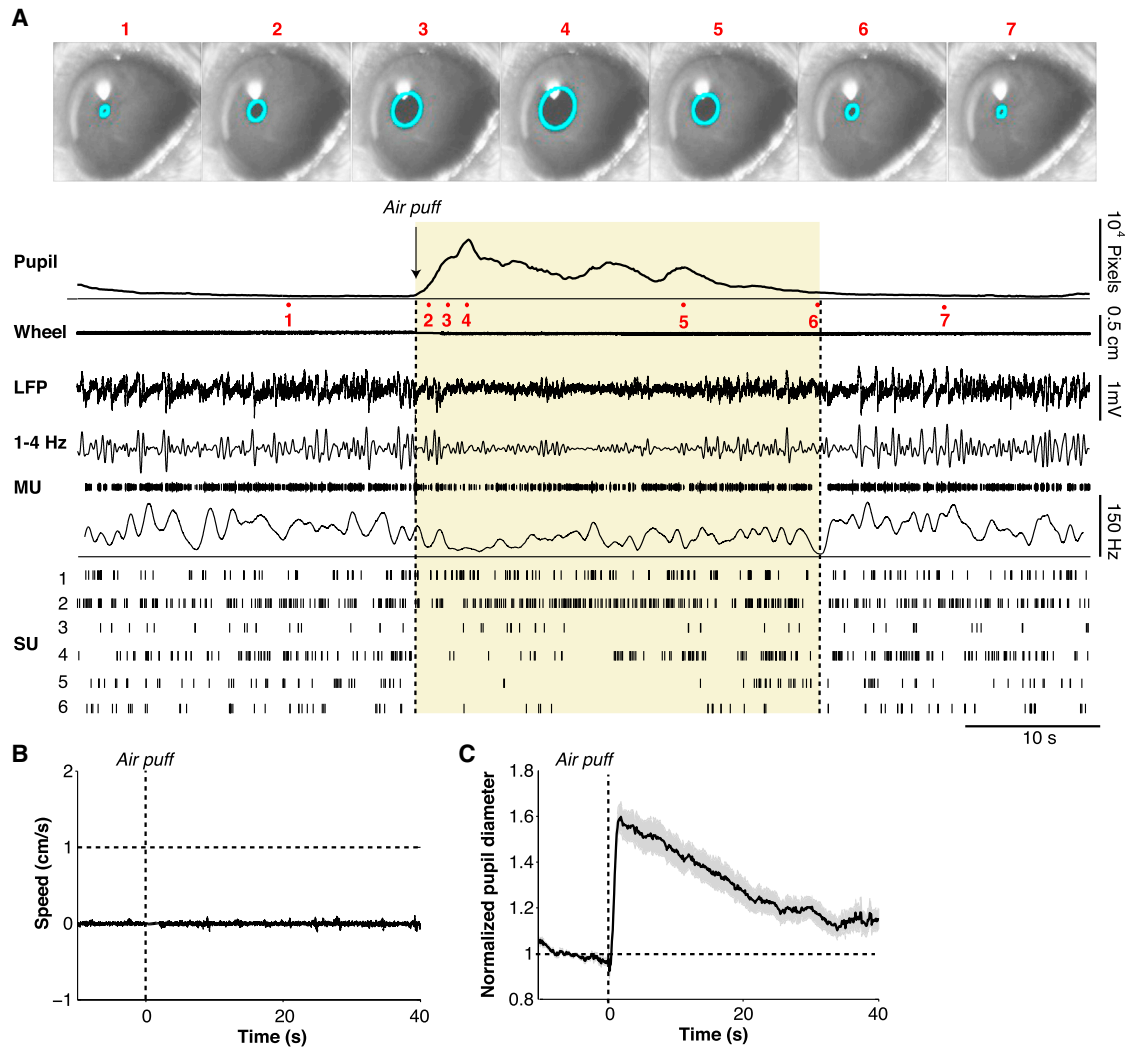


### Figure 5. Causal Induction of Arousal without Locomotion

(A) Example data from one experimental session. Video images captured of eye are shown for several time points (1–7). Average pupil diameter trace in pixels is shown as a function of time around air puff onset. Locomotion is shown as a linearized version of the wheel position. LFP recording is shown for one electrode, together with the 1–4 Hz filtered signal. A multiunit trace (MU) and associated spike density plot are shown for the same electrode. Single-unit traces (SU1–6) were isolated from three electrodes in L5/6 during this recording session. Shaded yellow area indicates period during which pupil was dilated, for demonstration purposes.

(B) Average locomotion speed as a function of time around the air puff.

(C) Average pupil diameter, normalized to pre-air-puff interval (–10 to 1 s before air puff), as a function of time. The SEMs were computed across sessions ( $n = 20$  in ten mice).

monitoring pupil diameter and performing simultaneous recordings of V1 LFPs and isolated single cells (Figure 5;  $n = 61$  cells in ten mice).

Delivery of the air puff reliably induced both arousal, as measured by pupil dilation, and changes in unit activity in the absence of locomotion (Figure 5A; Movie S2). Across sessions ( $n = 20$  sessions in ten mice), air puffs caused an average 1.6-fold increase in pupil diameter in the absence of locomotion (Figures 5B and 5C). This increase was similar in magnitude to the average increase in pupil diameter observed during locomotion (Figure 1C), suggesting a comparable level of arousal. We did

not find a significant correlation between trial number and the normalized pupil diameter (computed in the interval 1–4 s after the air puff; Spearman's  $\rho = -0.05 \pm 0.07$ ), or a difference between the first and last five trials ( $p = 0.63$ , Rank-Wilcoxon test), indicating little adaptation to air puffs within sessions.

### LFP Modulation by Induced Arousal

Our analysis of arousal periods following locomotion offset (Figure 2) predicts that a shift to an aroused state in the absence of locomotion should be accompanied by a decrease in low-frequency LFP power and an increase in gamma-band power.

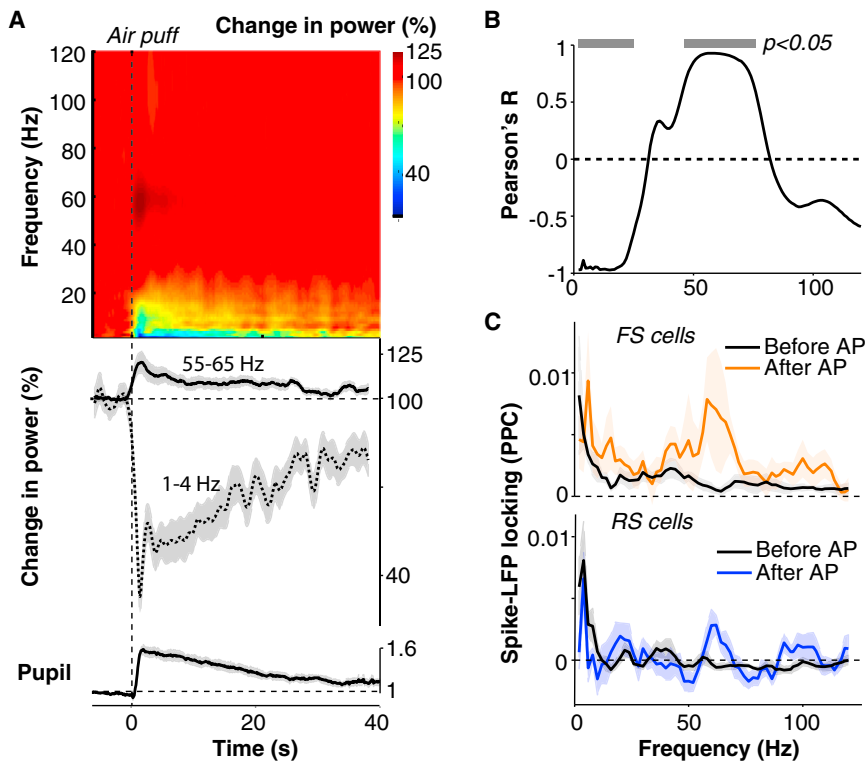


**Figure 6. Arousal Causes a Frequency Shift in V1 LFP Activity**

(A) Top: time-frequency representations of LFP signals around the air puff (AP). Base-10 log-transformed relative power, i.e., power at time  $t$  divided by average power in the interval preceding the air puff ( $-6$  to  $-1$  s),  $n = 45$  sites/ten mice. Middle: line plots of gamma and delta power, with shading representing SEM, across sites, around time of air puff. Bottom: pupil diameter trace, as in Figure 5C.

(B) Correlation of pupil diameter time course with LFP time course at various frequencies. Gray horizontal bars indicate significance at  $p < 0.05$ , linear regression analysis.

(C) Spike-field locking spectra (PPC) for FS (upper) and RS (lower) cells, separately for baseline before air puff (10 s) and period immediately after air puff (1–4 s). Shadings correspond to SEMs across cells. FS: 8/5; RS: 11/5 (#cells/#mice).

Indeed, we found that after the air puff the LFP showed a long-lasting, 2.5-fold decrease in low-frequency fluctuations comparable in magnitude to the locomotion effect (Figure 6A). The induced arousal also caused a 1.25-fold increase in gamma-band power. The pupil diameter time course showed a strong positive correlation with gamma-band power, and a negative correlation with low-frequency power (Figure 6B). The increase in gamma power was accompanied by a significant increase in the spike-LFP gamma phase-locking of both RS and FS cells and by a significant decrease in low-frequency RS locking (difference between FS and RS cells for before versus after air puff comparison n.s.; Figure 6C). Finally, we found that air puffs during locomotion periods did not induce a significant change in either low-frequency or gamma-band power, indicating that air puffs did not yield additional effects when the mouse was already in a state of heightened arousal (Figure S6). Together, these findings indicate that a shift to a state of high arousal without locomotion causes a decrease in low-frequency fluctuations and an increase in gamma-band fluctuations in V1.

#### Rate Modulation by Induced Arousal

We next investigated how firing rates were affected by the causal manipulation of arousal levels. Overall, we found that the air puff caused a significant, long-lasting decrease in spontaneous firing rates (Figures 7A and 7B). However, a small subpopulation of RS and FS cells showed elevated firing rates after the air puff (Figures 7A and 7C). Air puffs were particularly suppressive for RS cells if they had a high propensity to engage in irregular burst firing (Figure 7D; Experimental Procedures), but a similar relationship was not observed for FS cells (Figure 7D).

Individual neurons should show similar effects in response to naturally occurring and induced arousal. We therefore predicted that cells whose firing rates were suppressed by the induced arousal would likewise show suppression after locomotion offset, followed by gradual increases in firing rate over time as arousal levels spontaneously decreased (Figure 3). For this analysis, we selected only locomotion epochs that did not occur within 50 s of an air puff. We first defined the spontaneous-arousal modulation as the correlation between time after locomotion offset and firing, with positive values indicating that a cell was suppressed by arousal. We also defined the induced-arousal modulation in the interval after the air puff. We found that the spontaneous-arousal and induced-arousal modulations were significantly negatively correlated, demonstrating consistent effects of arousal on firing rate (Figure 7E).

The coordinated effects of induced arousal on firing rate and pupil diameter also predict that fluctuations in arousal should correlate on a trial-by-trial basis with firing rates. We predicted (more) negative correlations between pupil diameter and firing rates across trials for cells whose firing was on average suppressed by the air puff. Likewise, we predicted (more) positive correlations for cells whose firing was enhanced by the air puff. These predictions were supported by trial-by-trial correlation analysis (Figure 7F). Air puffs during locomotion periods did not induce a significant change in average firing rate, suggesting that air puffs did not have an additional suppressive effect when the mouse was already in a state of heightened arousal (Figure S6). Together, these results suggest that global arousal is associated with decreased spontaneous firing rates.

#### Arousal and Visual Encoding

To isolate the role of arousal in modulating single cell and population visual encoding, we administered air puffs randomly in combination with presentation of visual stimuli in a subset of experiments (Experimental Procedures). We then compared visual

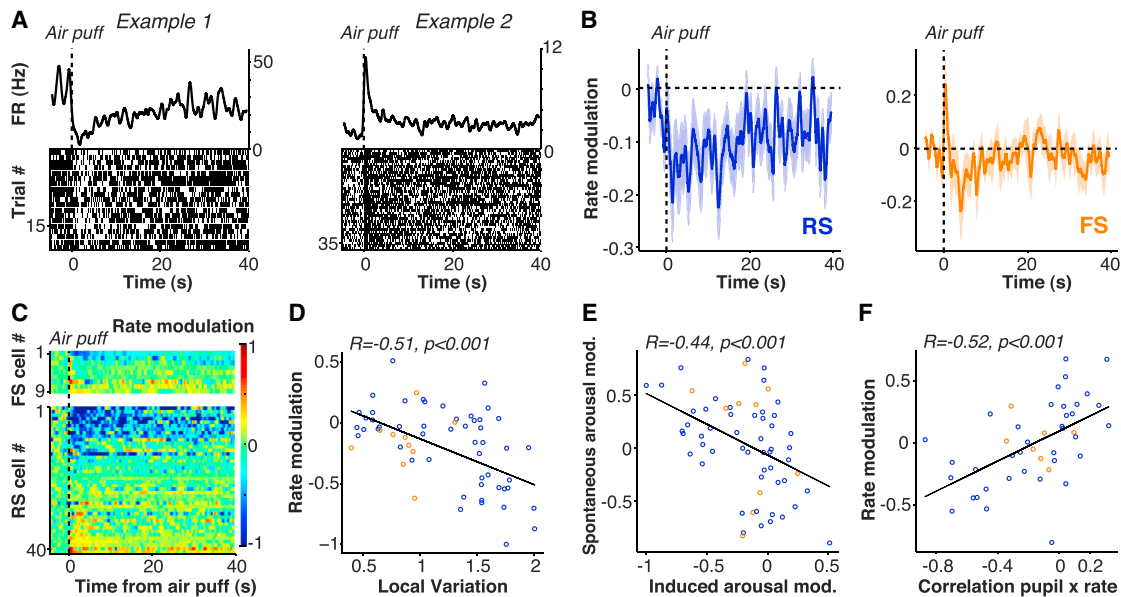


**Figure 7. Arousal Suppresses Firing Rates in V1**

(A) Raster plots and spike density traces (1 s windows with Gaussian kernel and SD of 250 ms) from two example (left: FS; right: RS) cells are shown as a function of time.

(B) Average modulation of firing rate, defined as  $[FR_{\text{post}} - FR_{\text{pre}}] / [FR_{\text{post}} - FR_{\text{pre}}]$  induced by the air puff for RS (blue) and FS (orange) cells, relative to 6 s prior to air puff. Mean  $\pm$  SEM of modulation in the interval after the air puff (1–4 s) for RS =  $-0.19 \pm 0.046$ ,  $p = 0.00046$ ,  $n = 51/9$  (#cells/#mice). FS:  $-0.14 \pm 0.074$ ,  $p = 0.084$ ,  $n = 10/6$ . The difference between FS and RS cells was not significant (Rank-Wilcoxon test;  $p = 0.87$ ).

(C) Rate modulation scores for all FS (upper) and RS (lower) cells as a function of time, relative to 6 s prior to air puff.

(D) Rate modulation index, comparing 1 to 4 s post-air puff to 6 s prior to air puff, as a function of local variation coefficient, a measure of firing regularity. High local variation values correspond to bursty cells and a local variation coefficient of 1 indicates Poisson-like firing (Experimental Procedures). RS cells:  $R = -0.57$ ,  $p = 0.00001$ ,  $n = 51/9$ ; FS cells:  $R = 0.13$ ,  $p = 0.71$ ,  $n = 10/6$  (#cells/#mice).

(E) Values on the x axis indicate induced-arousal rate modulation index (as in D). Values on the y axis indicate spontaneous-arousal modulation, calculated as the Spearman correlation of time after locomotion (>3 s) and firing rate.  $R = -0.47$ ,  $p = 0.000415$ ; NS:  $R = -0.32$ ,  $p = 0.36$ , difference RS and FS n.s., Fisher Z test.

(F) Rate modulation index (as in D) versus correlation of pupil diameter and firing rate across trials. Correlation of pupil and firing rate was defined over trials using the interval after the air puff (1–4 s). Pearson's  $R = 0.52$ ,  $p = 0.00033$ ,  $n = 45/7$ .

responses in the 10 s before the air puff with those in the 10 s after the air puff. Across the population of cells, we found a significant increase in SNRI following the induced arousal (Figures 8A and 8B). We also observed that induced arousal significantly decreased noise correlations (Figures 8A and 8C). These results indicate that arousal alone replicates the effects of locomotion on visual encoding, leading to an increase in the salience of visual responses by individual cells and decorrelating activity across the population.

## DISCUSSION

We examined the distinct contributions of arousal and locomotion to V1 activity and visual encoding using extracellular recording in combination with behavioral state monitoring and manipulation. Our data revealed that much of the change in V1 LFP power, spike-LFP phase-locking, and unit activity associated with locomotion is the result of increased arousal. We found that heightened arousal in the absence of locomotion has several cortical impacts: (1) a change in the temporal patterning of neural activity, comprising a reduction in low-frequency oscillations and an increase in gamma synchronization, (2) a net suppression of spontaneous firing rates, and (3) a change in visual encoding at

both the single-cell and population levels. In contrast, locomotion specifically contributes to an increase in RS and FS cell firing rates in anticipation of and during movement. Arousal state and motor activity thus have distinct roles in regulating activity in primary visual cortical circuits.

We found substantial differences in V1 activity between periods of quiescence and locomotion. This is consistent with several studies that used electrophysiology or calcium imaging in awake head-fixed rodents (Bennett et al., 2013; Fu et al., 2014; Keller et al., 2012; Lee et al., 2014; Niell and Stryker, 2010; Polack et al., 2013; Reimer et al., 2014; Saleem et al., 2013). However, previous results suggested that elevated RS cell firing during locomotion periods was not associated with locomotion, but was rather a modulation of visual responses (Bennett et al., 2013; Niell and Stryker, 2010). By focusing on state transition points, we were able to show that RS firing was strongly increased in anticipation of locomotion and during movement, even in the absence of visual stimulation. In contrast, causal induction of a state of high arousal caused a suppression of spontaneous firing rates, indicating that motor and arousal signals may have opposing effects on spontaneous spiking activity in V1. Studies in auditory cortex have found that firing rates of both RS and FS cells are suppressed by locomotion

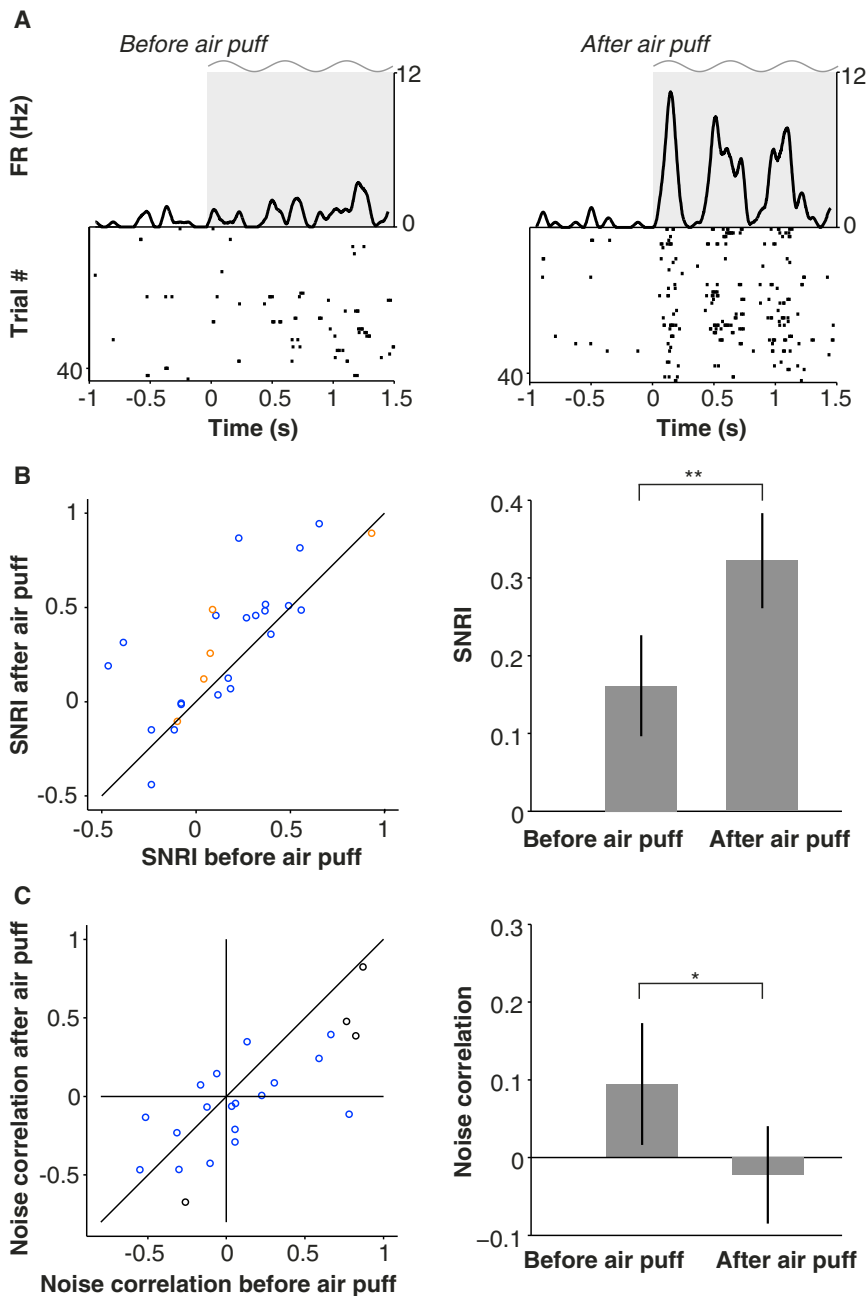


**Figure 8. Arousal Enhances Visual Encoding and Decreases Noise Correlations in V1**

(A) Raster plots of the visual responses of an example cell with associated firing rate density (computed using  $\pm 0.025$  s Gaussian kernels with SD of 0.0125) before (left) and after (right) air puff. Gray shading and sinusoid indicate visual stimulation.

(B) Plot of signal-to-noise ratio index (SNRI) for the 10 s interval before air puff (y axis) compared to 10 s interval after air puff (x axis). Population SNRI is shown at right, as mean  $\pm$  SEM ( $n = 25/8$ , #cells/#pairs).

(C) Noise correlation in the 10 s after air puff compared to the 10 s before air puff. Circles correspond to cell pairs (red = FS, blue = RS, black = FS/RS). Population average noise correlation is shown at right. (B and C)  $*p < 0.05$ ,  $**p < 0.01$ ,  $n = 22/4$  (#pairs/#mice), two-sided Rank-Wilcoxon test.

indicate that increased arousal levels and motor-related activity in V1 reliably precede the execution of motor output. Increased firing in anticipation of locomotion, consistent with motor planning or predictive coding (Keller et al., 2012; Saleem et al., 2013), could rely on top-down inputs from fronto-parietal circuits, in which many cells fire in anticipation of saccades and other movements (Bruce and Goldberg, 1985; Snyder et al., 1997). Indeed, recent work in mice has highlighted the existence of long-range inputs from frontal to striate cortex (Zhang et al., 2014) and motor cortical areas may also project to V1 or other visual areas (Miller and Vogt, 1984; Wang et al., 2011).

Distinct V1 cell populations exhibited different modulation around transition points. We observed enhanced signal-to-noise during locomotion for visual responses only in RS, putative excitatory cells but not in FS, putative inhibitory cells, potentially indicating cell-type specific regulation of visual encoding. Recent

(Schneider et al., 2014; Zhou et al., 2014), whereas studies in barrel cortex have shown that firing rates of RS and FS cells are unaffected and suppressed by whisking, respectively (Gentet et al., 2010, 2012; Schneider et al., 2014; Zhou et al., 2014). Thus, increased RS and FS firing during locomotion is likely specific to visual cortex and may be related to the necessity for integration of motor and visual signals to faithfully represent the outside world with respect to the animal's position (Keller et al., 2012; Saleem et al., 2013).

Firing rates and LFP power in the low (1–4 Hz) and gamma (55–65 Hz) ranges showed changes well in advance of the onset of locomotion, as did pupil diameter. These anticipatory changes

work has highlighted distinct patterns of state-dependent recruitment of different interneuron classes (Fu et al., 2014; Gentet et al., 2012; Polack et al., 2013; Reimer et al., 2014; Zhou et al., 2014). Notably, we found diversity within both the RS and FS cell populations in the trajectory of state-dependent changes in firing patterns at behavioral state transition points. Whereas most RS and FS cells were suppressed by arousal, a subset of both cell types instead showed enhanced firing. Firing rate suppression with arousal was particularly evident in bursting RS cells. Despite an overall reduction in firing rates, arousal was associated with enhanced phase locking of V1 neurons to gamma rhythms. FS cells were more strongly locked to LFP

gamma oscillations than RS cells, in agreement with the proposed role of FS interneurons in generating these oscillations (Cardin et al., 2009; Csicsvari et al., 2003; Sohal et al., 2009; Vinck et al., 2013; Whittington et al., 1995)

To robustly interpret the effect of arousal on firing rates, we focused on periods that were independent of motor anticipation or changes in velocity. An alternative approach would have been to regress out the influence of locomotion speed in a multivariate model to isolate the relationship between firing rate and pupil diameter, as the activity of a cell at any moment in time might potentially be well predicted by a model using both locomotion speed and pupil diameter. However, the relationship between speed and firing rate is not captured well by a linear model in the form of  $\text{Activity}(t) = a1 \cdot \text{speed}(t) + a2 \cdot \text{pupil\_diameter}(t)$ , because units fire in anticipation of speed changes during locomotion onsets, creating a non-linear relationship between locomotion speed and firing rate (Figure S8). An expression of the form  $\text{Activity}(t) = \sum_s a1(s) \cdot \text{speed}(t-s) + a2(s) \cdot \text{pupil\_diameter}(t-s)$ , which sums across various lags  $s$  and thereby coarsens the time resolution, is minimally required. Furthermore, although cells fire in anticipation of locomotion, their firing rates lag the offset in locomotion, indicating that the influence of locomotion speed at various time lags cannot be linearly summed. In addition, Saleem et al. (2013) found that the firing of many cells is nonlinearly related to concurrent locomotion speed. Regressing out the influence of locomotion speed in a multivariate model to isolate the relationship with pupil diameter would thus not necessarily ensure adequate regression of correlations between firing rate and locomotion. This would be problematic, given the complex relationship between pupil diameter and locomotion (Figure 1).

We took advantage of direct manipulations of behavioral state to probe the dynamic range of behavioral state-dependent cortical activity. Causal induction of arousal with the air puff stimulus initiated a shift from low to high frequencies in the cortical LFP. We found that induced arousal replicated the 2.5-fold reduction in 1–4 Hz fluctuations observed during locomotion periods. Low-frequency fluctuations increased only gradually after locomotion offset, with a strong linear relationship to the pupil diameter. Arousal alone therefore appears to account for the reduction in 1–4 Hz LFP power during locomotion periods. The observed linear relationship between pupil diameter and 1–4 Hz LFP power differs from recent work in which pupil diameter did not correlate with low-frequency membrane potential power, likely because only very small and short-lasting pupil fluctuations were considered (Reimer et al., 2014). LFP and firing rate changes were dissociated from one another during arousal periods, as the gradual increase in LFP low-frequency power and decrease in LFP gamma-band power were accompanied by a net increase in firing rates over the same period.

The effect of arousal on gamma-band LFP power in the absence of locomotion (~20% increase) was smaller than the increase in gamma-band LFP power during locomotion periods (~40% increase). Gamma-band power showed a similar adaptation during the locomotion period as firing rates, in contrast to 1–4 Hz power. A change in arousal might therefore not exclusively account for the increase in gamma-band power during locomotion periods, suggesting that locomotion might further amplify gamma-band oscil-

lations through the increased drive of local RS and FS cells (Cardin et al., 2009; Csicsvari et al., 2003; Sohal et al., 2009; Whittington et al., 1995). Previous work has linked noise correlations to intrinsic low-frequency fluctuations and a decrease in gamma-band oscillations (Harris and Thiele, 2011; Herrero et al., 2013; Mitchell et al., 2009; Womelsdorf et al., 2012). The effects of arousal observed here thus overlap with those of focused spatial attention in primates, where attention is associated with increased temporal patterning in the gamma band and decreased noise correlations (Cohen and Maunsell, 2009; Fries et al., 2001; Harris and Thiele, 2011; Mitchell et al., 2009).

State-dependent changes in visual encoding were highly correlated with arousal level across a wide range, suggesting extensive flexibility in the sensory processing operations of cortical circuits. An increase in the signal-to-noise ratio of visual responses in V1 has previously been reported for waking versus sleeping states (Livingstone and Hubel, 1981; Steriade et al., 2001), indicating possible regulation of visual sensitivity by overall arousal levels. In agreement with this idea, we found that states of high arousal were associated with increased signal-to-noise ratios and decreased noise correlations, indicating enhanced encoding of visual stimuli at both the single-cell and population levels. We found a strong trial-by-trial correlation between arousal, as measured by pupil diameter, and both measures of visual encoding, suggesting a dynamic system in which changes in arousal fine-tune the gain of visual responses in V1 on a moment-to-moment basis.

Lesion and stimulation studies have supported causal roles for several major neuromodulatory systems in controlling sleep-wake transitions and the temporal pattern of cortical activity, including norepinephrine and acetylcholine (Buzsaki et al., 1988; Carter et al., 2010; Constantinople and Bruno, 2011; Lee et al., 2014; Metherate et al., 1992; Munk et al., 1996; Pinto et al., 2013). Like arousal, neuromodulatory action desynchronizes the cortex, promotes gamma oscillations, and changes sensory encoding (Carter et al., 2010; Fu et al., 2014; Harris and Thiele, 2011; Munk et al., 1996; Pinto et al., 2013; Steriade et al., 1993). Noradrenergic blockade of awake mouse V1 eliminates the depolarization and elevated firing associated with locomotion (Polack et al., 2013). Recent evidence also points to the involvement of the mesencephalic locomotor region, a cholinergic brainstem nucleus, in the control of locomotion and regulation of V1 activity patterns and visual responses (Lee et al., 2014). In addition, cholinergic afferents from the basal forebrain nucleus of the diagonal band of Broca selectively target V1 interneurons involved in locomotion-related changes in firing rates (Fu et al., 2014). Arousal effects observed in V1 during waking state transitions are thus likely involve complex interactions between multiple neuromodulatory systems.

In summary, our data show that activity in mouse visual cortex during wakefulness is differentially regulated by arousal and motor signals. We find a complex interaction between internally generated cortical states and visual inputs. Arousal restructures spontaneous cortical activity and promotes fast gamma-band oscillations, which may be optimal for synchronized, bottom-up routing of sensory signals (Busse et al., 2011; Fries et al., 2001; van Kerkoerle et al., 2014; Womelsdorf et al., 2012). This shift in the mode of cortical operation also strongly increases

the signal-to-noise ratio of visual representations. The interplay between arousal level, motor activity, and sensory input may contribute to the functional flexibility of cortical circuits.

## EXPERIMENTAL PROCEDURES

### Animals, Headpost Surgery, and Wheel Training

All animal handling was performed in accordance with guidelines approved by the Yale Institutional Animal Care and Use Committee and federal guide. We handled 4- to 6-month-old male wild-type mice for 5–10 min/day in the 5 days prior to the headpost surgery. Following surgery, mice were allowed to recover for 3–5 days before wheel training commenced. Mice were head-fixed on the wheel for increasing intervals on each successive day, and were trained on the wheel for up to 7 days or until they exhibited robust bouts of running activity during each session.

### Electrophysiology

Simultaneous recordings of isolated single units and LFPs were made from multiple sites throughout layers 2–6 of V1 in awake mice. Recordings were made both during baseline periods, in which the LCD monitor displayed an isoluminant gray screen, and during visual stimulation periods, in which drifting gratings were presented for 1.5–2 s, interspersed with the presentation of an isoluminant gray screen in the ITI. Infrared camera recordings were made of the eye ipsilateral to the craniotomy to measure pupil diameter. In a first set of experiments, we analyzed spontaneous transitions in locomotion, arousal, and cortical activity. In a second set of experiments, a small tube was positioned behind the mice's head and air puffs were delivered to the body of the mouse during quiescent periods.

### Locomotion and Pupil Diameter Analysis

A change-point detection algorithm was used to detect statistical differences in the distribution of locomotion velocities across time in order to identify locomotion on- and offset. Pupil diameter was extracted from gray-scale video frames of 800 × 600 pixels at 10 Hz. Fuzzy c-means clustering was used to identify a cluster of pixels corresponding to the pupil, and the pupil was extracted using edge detection and ellipsoid fitting.

### Spectral LFP and Spike-LFP Analyses

LFP power spectral density was estimated at each time point using seven cycles of LFP data per frequency and a Hann taper. We then performed smoothing of the spectra with rectangular box car windows such that always 4 s of data were used to estimate power at a certain time point. For computing LFP spectra during visual stimulation, we divided the data in 500 ms segments and used multitapering with  $\pm 4$  Hz smoothing.

Spike-field locking was computed using the pairwise phase consistency (Vinck et al., 2012, 2013), a measure of phase consistency that is not biased by the number of spikes. Spike-LFP phases were computed for each spike and frequency separately by using discrete Fourier transform with Hanning taper of an LFP segment of length  $9/f$ , where  $f$  is the frequency of interest.

### Noise Correlations

For each unique visual stimulus, firing rates were computed for the entire stimulus period, and Z scored across (at least three) presentations of that stimulus. We then concatenated the Z-scored firing rates across the different unique stimuli, and computed the Pearson's correlation coefficient.

### Computation of Modulation and SNRI

Computation of firing rate modulation and SNRI (signal-to-noise ratio index) was always performed as  $y = [FR_1 - FR_2]/[FR_1 + FR_2]$ .

### Quantification of Burstiness

The propensity to engage in burst firing was quantified using the coefficient of local variation (LV; Shinomoto et al., 2009), which is robust against non-stationarities in firing rates. This measure correlates strongly with the log fraction of ISIs between 2 and 10 ms over the fraction of ISIs between 10 and 100 ms, i.e.,  $\text{Log}(|\text{ISI}_{\text{short}}|/|\text{ISI}_{\text{long}}|)$  (Pearson's  $R = 0.84$ ,  $p = 7 \times 10^{-15}$ , Figure S7).

### Spike Densities

Instantaneous firing rate was computed by convolving the spike trains either with a rectangular kernel or a Gaussian smoothing kernel. For tracking longer-lasting changes in firing rate around state transition points (Figures 1, 3, and 7), relatively long smoothing kernels ( $\pm 500$  ms Gaussian kernels, with SD of 250 ms) were used. For depicting neuronal responses to visual stimuli (Figures 4 and 8), short smoothing kernels ( $\pm 25$  ms Gaussian kernels, with SD of 12.5 ms) were used.

## SUPPLEMENTAL INFORMATION

Supplemental Information includes Supplemental Experimental Procedures, eight figures, and two movies and can be found with this article online at <http://dx.doi.org/10.1016/j.neuron.2015.03.028>.

## AUTHOR CONTRIBUTIONS

M.V., R.B.B., U.K., and J.A.C. designed research. R.B.B., M.V., and J.A.C. conducted experiments. U.K. and J.A.C. developed hardware. M.V. analyzed data. M.V. and J.A.C. wrote the manuscript.

## ACKNOWLEDGMENTS

This research was supported by a NARSAD Young Investigator award, an Alfred P. Sloan Fellowship award, a Whitehall grant, a Klingenstein fellowship award, a McKnight Scholar award, and NIH/NEI grants R00 EY018407 and R01 EY022951 (to J.A.C.), a Rubicon Grant (Netherlands Organization for Science; to M.V.), a Jane Coffin Childs Fund fellowship award (to R.B.B.), and a NARSAD Young Investigator award (to U.K.). We thank James Mossner and Hyun Lee for technical support. We also thank the main developers of M-Clust (D. Redish), KlustaKwik (K. Harris), and FieldTrip (R. Oostenveld) for free use of their software. We thank M.J. Higley for comments on the manuscript.

Received: December 3, 2014

Revised: February 5, 2015

Accepted: March 11, 2015

Published: April 16, 2015

## REFERENCES

- Aston-Jones, G., and Cohen, J.D. (2005). An integrative theory of locus coeruleus-norepinephrine function: adaptive gain and optimal performance. *Annu. Rev. Neurosci.* 28, 403–450.
- Bennett, C., Arroyo, S., and Hestrin, S. (2013). Subthreshold mechanisms underlying state-dependent modulation of visual responses. *Neuron* 80, 350–357.
- Berger, H. (1929). Über das elektroencephalogramm des menschen. *Eur. Arch. Psychiatry Clin. Neurosci.* 87, 527–570.
- Bruce, C.J., and Goldberg, M.E. (1985). Primate frontal eye fields. I. Single neurons discharging before saccades. *J. Neurophysiol.* 53, 603–635.
- Busse, L., Ayaz, A., Dhruv, N.T., Katzner, S., Saleem, A.B., Schölvinck, M.L., Zaharia, A.D., and Carandini, M. (2011). The detection of visual contrast in the behaving mouse. *J. Neurosci.* 31, 11351–11361.
- Buzsáki, G., Bickford, R.G., Ponomareff, G., Thal, L.J., Mandel, R., and Gage, F.H. (1988). Nucleus basalis and thalamic control of neocortical activity in the freely moving rat. *J. Neurosci.* 8, 4007–4026.
- Cardin, J.A., Carlén, M., Meletis, K., Knoblich, U., Zhang, F., Deisseroth, K., Tsai, L.H., and Moore, C.I. (2009). Driving fast-spiking cells induces gamma rhythm and controls sensory responses. *Nature* 459, 663–667.
- Carter, M.E., Yizhar, O., Chikahisa, S., Nguyen, H., Adamantidis, A., Nishino, S., Deisseroth, K., and de Lecea, L. (2010). Tuning arousal with optogenetic modulation of locus coeruleus neurons. *Nat. Neurosci.* 13, 1526–1533.
- Civillico, E.F., and Contreras, D. (2012). Spatiotemporal properties of sensory responses in vivo are strongly dependent on network context. *Front. Syst. Neurosci.* 6, 25.

- Cohen, M.R., and Kohn, A. (2011). Measuring and interpreting neuronal correlations. *Nat. Neurosci.* *14*, 811–819.
- Cohen, M.R., and Maunsell, J.H. (2009). Attention improves performance primarily by reducing interneuronal correlations. *Nat. Neurosci.* *12*, 1594–1600.
- Constantinople, C.M., and Bruno, R.M. (2011). Effects and mechanisms of wakefulness on local cortical networks. *Neuron* *69*, 1061–1068.
- Contreras, D., Timofeev, I., and Steriade, M. (1996). Mechanisms of long-lasting hyperpolarizations underlying slow sleep oscillations in cat corticothalamic networks. *J. Physiol.* *494*, 251–264.
- Crochet, S., and Petersen, C.C. (2006). Correlating whisker behavior with membrane potential in barrel cortex of awake mice. *Nat. Neurosci.* *9*, 608–610.
- Csicsvari, J., Jamieson, B., Wise, K.D., and Buzsáki, G. (2003). Mechanisms of gamma oscillations in the hippocampus of the behaving rat. *Neuron* *37*, 311–322.
- Destexhe, A., Contreras, D., and Steriade, M. (1999). Spatiotemporal analysis of local field potentials and unit discharges in cat cerebral cortex during natural wake and sleep states. *J. Neurosci.* *19*, 4595–4608.
- Ecker, A.S., Berens, P., Keliris, G.A., Bethge, M., Logothetis, N.K., and Tolias, A.S. (2010). Decorrelated neuronal firing in cortical microcircuits. *Science* *327*, 584–587.
- Eldar, E., Cohen, J.D., and Niv, Y. (2013). The effects of neural gain on attention and learning. *Nat. Neurosci.* *16*, 1146–1153.
- Fries, P., Reynolds, J.H., Rorie, A.E., and Desimone, R. (2001). Modulation of oscillatory neuronal synchronization by selective visual attention. *Science* *291*, 1560–1563.
- Fu, Y., Tucciarone, J.M., Espinosa, J.S., Sheng, N., Darcy, D.P., Nicoll, R.A., Huang, Z.J., and Stryker, M.P. (2014). A cortical circuit for gain control by behavioral state. *Cell* *156*, 1139–1152.
- Gettet, L.J., Avermann, M., Matyas, F., Staiger, J.F., and Petersen, C.C. (2010). Membrane potential dynamics of GABAergic neurons in the barrel cortex of behaving mice. *Neuron* *65*, 422–435.
- Gettet, L.J., Kremer, Y., Taniguchi, H., Huang, Z.J., Staiger, J.F., and Petersen, C.C. (2012). Unique functional properties of somatostatin-expressing GABAergic neurons in mouse barrel cortex. *Nat. Neurosci.* *15*, 607–612.
- Gilzenrat, M.S., Nieuwenhuis, S., Jepma, M., and Cohen, J.D. (2010). Pupil diameter tracks changes in control state predicted by the adaptive gain theory of locus coeruleus function. *Cogn. Affect. Behav. Neurosci.* *10*, 252–269.
- Guo, Z.V., Li, N., Huber, D., Ophir, E., Gutnisky, D., Ting, J.T., Feng, G., and Svoboda, K. (2014). Flow of cortical activity underlying a tactile decision in mice. *Neuron* *81*, 179–194.
- Haider, B., Häusser, M., and Carandini, M. (2013). Inhibition dominates sensory responses in the awake cortex. *Nature* *493*, 97–100.
- Harris, K.D., and Thiele, A. (2011). Cortical state and attention. *Nat. Rev. Neurosci.* *12*, 509–523.
- Hasenstaub, A., Sachdev, R.N., and McCormick, D.A. (2007). State changes rapidly modulate cortical neuronal responsiveness. *J. Neurosci.* *27*, 9607–9622.
- Herrero, J.L., Gieselmann, M.A., Sanayei, M., and Thiele, A. (2013). Attention-induced variance and noise correlation reduction in macaque V1 is mediated by NMDA receptors. *Neuron* *78*, 729–739.
- Keller, G.B., Bonhoeffer, T., and Hübener, M. (2012). Sensorimotor mismatch signals in primary visual cortex of the behaving mouse. *Neuron* *74*, 809–815.
- Lee, S., Kruglikov, I., Huang, Z.J., Fishell, G., and Rudy, B. (2013). A disinhibitory circuit mediates motor integration in the somatosensory cortex. *Nat. Neurosci.* *16*, 1662–1670.
- Lee, A.M., Hoy, J.L., Bonci, A., Wilbrecht, L., Stryker, M.P., and Niell, C.M. (2014). Identification of a brainstem circuit regulating visual cortical state in parallel with locomotion. *Neuron* *83*, 455–466.
- Livingstone, M.S., and Hubel, D.H. (1981). Effects of sleep and arousal on the processing of visual information in the cat. *Nature* *291*, 554–561.
- McAdams, C.J., and Maunsell, J.H. (1999). Effects of attention on the reliability of individual neurons in monkey visual cortex. *Neuron* *23*, 765–773.
- McCormick, D.A., and Bal, T. (1997). Sleep and arousal: thalamocortical mechanisms. *Annu. Rev. Neurosci.* *20*, 185–215.
- Metherate, R., Cox, C.L., and Ashe, J.H. (1992). Cellular bases of neocortical activation: modulation of neural oscillations by the nucleus basalis and endogenous acetylcholine. *J. Neurosci.* *12*, 4701–4711.
- Miller, M.W., and Vogt, B.A. (1984). Direct connections of rat visual cortex with sensory, motor, and association cortices. *J. Comp. Neurol.* *226*, 184–202.
- Mitchell, J.F., Sundberg, K.A., and Reynolds, J.H. (2009). Spatial attention decorrelates intrinsic activity fluctuations in macaque area V4. *Neuron* *63*, 879–888.
- Munk, M.H., Roelfsema, P.R., König, P., Engel, A.K., and Singer, W. (1996). Role of reticular activation in the modulation of intracortical synchronization. *Science* *272*, 271–274.
- Niell, C.M., and Stryker, M.P. (2010). Modulation of visual responses by behavioral state in mouse visual cortex. *Neuron* *65*, 472–479.
- Olshausen, B.A., and Field, D.J. (1996). Emergence of simple-cell receptive field properties by learning a sparse code for natural images. *Nature* *381*, 607–609.
- Pinto, L., Goard, M.J., Estandian, D., Xu, M., Kwan, A.C., Lee, S.H., Harrison, T.C., Feng, G., and Dan, Y. (2013). Fast modulation of visual perception by basal forebrain cholinergic neurons. *Nat. Neurosci.* *16*, 1857–1863.
- Polack, P.O., Friedman, J., and Golshani, P. (2013). Cellular mechanisms of brain state-dependent gain modulation in visual cortex. *Nat. Neurosci.* *16*, 1331–1339.
- Pouget, A., Dayan, P., and Zemel, R. (2000). Information processing with population codes. *Nat. Rev. Neurosci.* *1*, 125–132.
- Reimer, J., Froudarakis, E., Cadwell, C.R., Yatsenko, D., Denfield, G.H., and Tolias, A.S. (2014). Pupil fluctuations track fast switching of cortical states during quiet wakefulness. *Neuron* *84*, 355–362.
- Saleem, A.B., Ayaz, A., Jeffery, K.J., Harris, K.D., and Carandini, M. (2013). Integration of visual motion and locomotion in mouse visual cortex. *Nat. Neurosci.* *16*, 1864–1869.
- Schneider, D.M., Nelson, A., and Mooney, R. (2014). A synaptic and circuit basis for corollary discharge in the auditory cortex. *Nature* *513*, 189–194.
- Shinomoto, S., Kim, H., Shimokawa, T., Matsuno, N., Funahashi, S., Shima, K., Fujita, I., Tamura, H., Doi, T., Kawano, K., et al. (2009). Relating neuronal firing patterns to functional differentiation of cerebral cortex. *PLoS Comput. Biol.* *5*, e1000433.
- Snyder, L.H., Batista, A.P., and Andersen, R.A. (1997). Coding of intention in the posterior parietal cortex. *Nature* *386*, 167–170.
- Sohal, V.S., Zhang, F., Yizhar, O., and Deisseroth, K. (2009). Parvalbumin neurons and gamma rhythms enhance cortical circuit performance. *Nature* *459*, 698–702.
- Steriade, M., McCormick, D.A., and Sejnowski, T.J. (1993). Thalamocortical oscillations in the sleeping and aroused brain. *Science* *262*, 679–685.
- Steriade, M., Timofeev, I., and Grenier, F. (2001). Natural waking and sleep states: a view from inside neocortical neurons. *J. Neurophysiol.* *85*, 1969–1985.
- van Kerkoerle, T., Self, M.W., Dagnino, B., Gariel-Mathis, M.A., Poort, J., van der Togt, C., and Roelfsema, P.R. (2014). Alpha and gamma oscillations characterize feedback and feedforward processing in monkey visual cortex. *Proc. Natl. Acad. Sci. USA* *111*, 14332–14341.
- Vinck, M., Battaglia, F.P., Womelsdorf, T., and Pennartz, C. (2012). Improved measures of phase-coupling between spikes and the Local Field Potential. *J. Comput. Neurosci.* *33*, 53–75.
- Vinck, M., Womelsdorf, T., Buffalo, E.A., Desimone, R., and Fries, P. (2013). Attentional modulation of cell-class-specific gamma-band synchronization in awake monkey area v4. *Neuron* *80*, 1077–1089.

- Wang, Q., Gao, E., and Burkhalter, A. (2011). Gateways of ventral and dorsal streams in mouse visual cortex. *J. Neurosci.* *31*, 1905–1918.
- Whittington, M.A., Traub, R.D., and Jefferys, J.G. (1995). Synchronized oscillations in interneuron networks driven by metabotropic glutamate receptor activation. *Nature* *373*, 612–615.
- Womelsdorf, T., Lima, B., Vinck, M., Oostenveld, R., Singer, W., Neuenschwander, S., and Fries, P. (2012). Orientation selectivity and noise correlation in awake monkey area V1 are modulated by the gamma cycle. *Proc. Natl. Acad. Sci. USA* *109*, 4302–4307.
- Zagha, E., Casale, A.E., Sachdev, R.N., McGinley, M.J., and McCormick, D.A. (2013). Motor cortex feedback influences sensory processing by modulating network state. *Neuron* *79*, 567–578.
- Zhang, S., Xu, M., Kamigaki, T., Hoang Do, J.P., Chang, W.C., Jenvay, S., Miyamichi, K., Luo, L., and Dan, Y. (2014). Selective attention. Long-range and local circuits for top-down modulation of visual cortex processing. *Science* *345*, 660–665.
- Zhou, M., Liang, F., Xiong, X.R., Li, L., Li, H., Xiao, Z., Tao, H.W., and Zhang, L.I. (2014). Scaling down of balanced excitation and inhibition by active behavioral states in auditory cortex. *Nat. Neurosci.* *17*, 841–850.